PNAS RESEARCH ARTICLE | BIOPHYSICS AND COMPUTATIONAL BIOLOGY

Activity-driven chromatin organization during interphase: Compaction, segregation, and entanglement suppression

Brian Chan[a] and Michael Rubinstein[a,b,c,d,e,1]

Edited by Steve Granick, University of Massachusetts at Amherst, Amherst, MA; received January 26, 2024; accepted April 17, 2024

In mammalian cells, the cohesin protein complex is believed to translocate along chromatin during interphase to form dynamic loops through a process called active loop extrusion. Chromosome conformation capture and imaging experiments have suggested that chromatin adopts a compact structure with limited interpenetration between chromosomes and between chromosomal sections. We developed a theory demonstrating that active loop extrusion causes the apparent fractal dimension of chromatin to cross-over between two and four at contour lengths on the order of 30 kilo-base pairs. The anomalously high fractal dimension $D = 4$ is due to the inability of extruded loops to fully relax during active extrusion. Compaction on longer contour length scales extends within topologically associated domains (TADs), facilitating gene regulation by distal elements. Extrusion-induced compaction segregates TADs such that overlaps between TADs are reduced to less than 35% and increases the entanglement strand of chromatin by up to a factor of 50 to several Mega-base pairs. Furthermore, active loop extrusion couples cohesin motion to chromatin conformations formed by previously extruding cohesins and causes the mean square displacement of chromatin loci during lag times (Δt) longer than tens of minutes to be proportional to $\Delta t^{1/3}$. We validate our results with hybrid molecular dynamics—Monte Carlo simulations and show that our theory is consistent with experimental data. This work provides a theoretical basis for the compact organization of interphase chromatin, explaining the physical reason for TAD segregation and suppression of chromatin entanglements which contribute to efficient gene regulation.

loop extrusion | polymer physics | chromatin organization | active matter

Significance

During interphase, cells must compact chromatin such that gene promoters and their regulatory elements frequently contact each other in space. However, cells also need to insulate promoters from regulatory elements in other genomic sections. Using polymer physics theory and computer simulations, we propose that the cohesin protein complex actively extrudes chromatin into topologically associated domains (TADs) with an anomalously high fractal dimension of $D \approx 4$ while suppressing spatial overlap between different TADs. Our model suggests that the fast kinetics of active loop extrusion compared to the slow relaxation of chromatin loops maintains a dense chromatin organization. This work presents a physical framework explaining how cohesin contributes to effective transcriptional regulation.

Gene transcription during interphase can be regulated by spatial colocalization of promoters with enhancers or silencers located up to hundreds of kilo-base pairs (kbp) away (1) (Fig. 1*A*). These distal regulatory elements frequently act on genes within the same topologically associated domain (TAD) (2–4). TADs are continuous sections of chromatin that preferentially associate in space, identified by squares along the main diagonal of Hi-C contact maps (5, 6). One model for TAD formation is loop extrusion, in which the cohesin protein complex threads chromatin into growing loops until stopped by the CCCTC-binding factor (CTCF) at TAD boundaries (7–10) (Fig. 1*B*).

We consider active loop extrusion, in which cohesin uses adenosine triphospate (ATP) to move in biased directions toward domain boundaries (7–9, 11, 12). Active processes that consume energy are widespread throughout the cell and are known to modify the conformation and dynamics of different biopolymers, including chromatin. In general, ATP depletion decreases the diffusion constant of chromosomal loci (13) and eliminates their coherent dynamics, in which loci displacements correlate with those of other loci in close spatial proximity (14–16). A well-known example of an active process on chromatin is transcription, in which RNA Polymerase II (RNAPII) produces mRNA molecules from a DNA template (17–19) (Fig. 1*A*). In contrast to loop extrusion, RNAPII translocates at slower rates (0.01 to 0.1 kbp per second) compared to cohesin (0.1 to 1 kbp per second) and does not hold two chromatin loci together (20–24).

To effectively modulate transcription, promoters and distal regulatory elements such as enhancers and silencers should frequently come into physical contact. In other words, the contact probability $P(s)$ must decay slowly with the genomic distance s between them. Hi-C and Micro-C experiments have shown at least three power law scaling regimes for contact probabilities (Fig. 2), each characterized by $P(s) \sim s^{-\gamma_i}$, where $\sim$ indicates proportionality and the subscript i indicates different regimes. The three regimes typically have $1 \leq \gamma_1 \leq 1.5$, $\gamma_2 \approx 0.75$, and $1 \leq \gamma_3 \leq 1.5$ (5, 8, 25–32). The crossovers between these three regimes vary between experiments and are not well defined in part due to the ranges in observed scaling exponents. However, the crossover between γ_1 and γ_2 is typically on the order of 30 to 50 kbp, and the crossover between γ_2 and γ_3 is typically on the order

Author affiliations: [a]Department of Biomedical Engineering, Duke University, Durham, NC 27708; [b]Thomas Lord Department of Mechanical Engineering and Materials Science, Duke University, Durham, NC 27708; [c]Department of Physics, Duke University, Durham, NC 27708; [d]Department of Chemistry, Duke University, Durham, NC 27708; and [e]World Premier International Research Center Initiative–Institute for Chemical Reaction Design and Discovery, Hokkaido University, Sapporo 001-0021, Japan

Author contributions: B.C. and M.R. designed research; B.C. performed research; B.C. and M.R. analyzed data; and B.C. and M.R. wrote the paper.

The authors declare no competing interest.

This article is a PNAS Direct Submission.

[1]To whom correspondence may be addressed. Email: michael.rubinstein@duke.edu.

This article contains supporting information online at https://www.pnas.org/lookup/suppl/doi:10.1073/pnas.2401494121/-/DCSupplemental.

Published May 16, 2024.

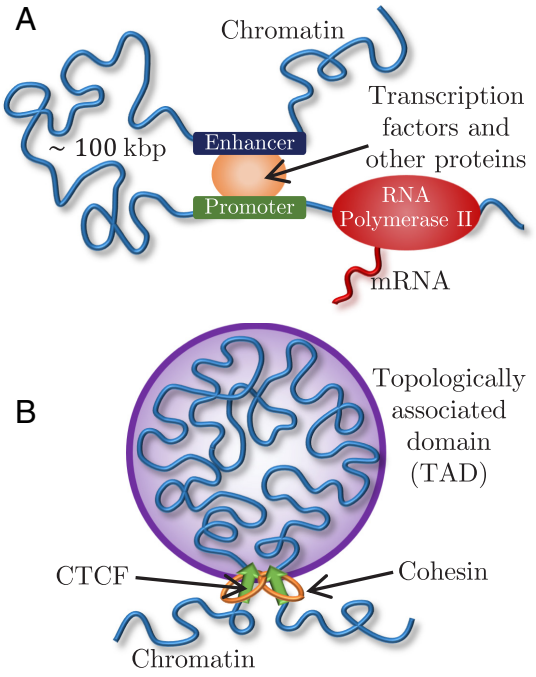

Fig. 1. Active processes on chromatin. (*A*) Eukaryotic transcription by RNAPII regulated by an enhancer–promoter interaction and TFs. (*B*) Active loop extrusion by cohesin forms TADs anchored by CTCF proteins.

of 200 to 500 kbp. Within a mean-field approximation $\gamma_i \approx 3/D_i$, where D_i is the fractal dimension (33). Fractal dimension describes how the mass m of an object grows with its physical size r such that $m \sim r^D$ (34). Mapping γ to fractal dimension yields $2 \leq D_1 \leq 3$ for the first regime, $D_2 \approx 4$ for the second, and $2 \leq D_3 \leq 3$ for the third. The second scaling regime occurs on genomic length scales on the order of a typical TAD (35, 36). Depleting chromatin-bound cohesins increases γ_2, suggesting that loop extrusion compacts chromatin on the scale of TADs by increasing its fractal dimension (5, 25, 37). Furthermore, experimental evidence suggests that cohesins assist in efficient target search by transcription factors (TFs) and regulate transcriptional bursting probabilities (32, 38, 39), which hints at a connection between loop extrusion, a window of decreased γ, and transcriptional regulation.

Cells must ensure that regulatory elements do not act on off-target genes, such as those in other TADs. Superresolution imaging suggests that neighboring TADs are spatially segregated (39–41). We argue that the increase in fractal dimension due to active loop extrusion would suppress overlaps between chromatin

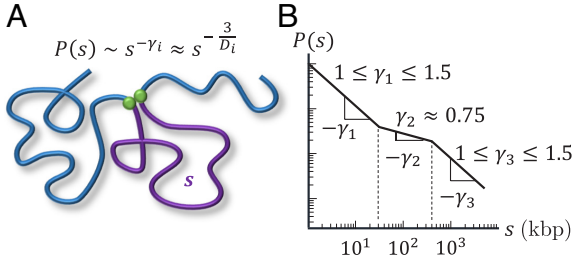

Fig. 2. Contact probabilities in interphase chromatin. (*A*) Schematic of a contact between two loci (green circles) separated by genomic distance s (purple curve). The contact probability between the two green loci $P(s)$ is proportional to a power law $P(s) \sim s^{-\gamma_i}$ where the subscript i indicates a specific regime. $\gamma_i \approx 3/D_i$ within a mean-field approximation, where D_i is the fractal dimension. (*B*) Schematic plot of the average contact probability $P(s)$ for chromatin as a function of genomic separation s with three scaling regimes on a log–log scale.

sections, where we define the overlap parameter as the number of chromatin sections of similar genomic lengths sharing the same volume (34). The entanglement length is a characteristic scale along the polymer above which topological constraints that prevent strand crossing dominate dynamic properties (34). An estimate of this entanglement is the strand length for which the overlap parameter is ~10. If chromatin were to adopt a random walk conformation with $D \approx 2$ between entanglements, the entanglement genomic length in the absence of activity and looping $N_{e,passive}$ would be 50 to 100 kbp (33, 42–44). However, this is in contrast to evidence that chromosomes and chromatin compartments do not intermingle extensively (45). We argue that extruded chromatin loops are not equilibrated and that the kinetics of active loop extrusion cause an increase of fractal dimension in compact loops and suppress entanglements by two orders of magnitude.

Several equilibrium polymer models are consistent with fractal dimensions larger than $D \approx 2$ (Fig. 3): i) a crumpled polymer with an exponential distribution of equilibrated loops (CPEL—Fig. 3*A*) (44, 46), ii) the fractal loopy globule (FLG) model for a melt of nonconcatenated ring polymers (Fig. 3*B*) (47), and iii) a ring polymer in an array of fixed topological obstacles, which can be mapped onto double folded lattice animals (DFLA—Fig. 3*C*) (48, 49). In CPEL, looped and unlooped chromatin sections have $D \approx 2$ (Fig. 3*A*). Loops shorten the effective contour length between genomic loci, causing a higher apparent fractal dimension on scales larger than the average loop length. Additional mass within loops contributes to entanglement dilution as in bottlebrush polymer systems (50). The FLG describes a crossover between fractal dimensions of $D \approx 2$ and $D \approx 3$ at the entanglement length smaller than a single ring such that loopy polymer sections maintain a constant degree of overlap with each other on all larger length scales (Fig. 3*B*) with large overlap parameter ~10. In DFLA, polymers have $D \approx 2$ on the smallest length scales as well (Fig. 3*C*). Double folds of ring polymers caused by their topological interactions with fixed networks produce lattice animal structures, resulting in $D \approx 4$ above the scale of the typical fold or loop. This regime extends until density saturation, above which $D \approx 3$.

CPEL, FLG, and DFLA are all equilibrium models, while our model explicitly considers nonequilibrium activity. Our model of active loop extrusion suggests that a crossover from $D \approx 2$ to $D \approx 4$ occurs on genomic lengths smaller than a typical loop extruded by a loop extruding protein. We argue that this compaction is a nonequilibrium process that occurs due to the fast kinetics of loop extrusion in comparison with loop relaxation. A random walk conformation of looped sections with $D \approx 2$ is recovered above the length scales of an average loop (Fig. 3*D*). Compaction by loop extrusion suppresses entanglements. The range of the applicability of our model depends on the interplay between the extrusion velocity and chromatin relaxation rate, which have yet to be resolved experimentally. As described below, we suggest that active loop extrusion significantly modifies chromatin conformation given the observed cohesin extrusion speeds and chromatin dynamics.

The main parameters used to describe active loop extrusion are processivity and separation. Processivity λ is the average genomic length extruded by an unobstructed cohesin. Separation d is the average genomic length between chromatin-bound cohesins or the inverse of the linear density of cohesins. Both λ and d are predicted to be on the order of 200 kbp, suggesting limited loop nesting (7, 11, 51). Extrusion velocity v_{ex} is the average genomic length extruded per unit time and is equal to the processivity divided by the average residence time of an unobstructed cohesin τ_{res}. v_{ex} is on the order of 0.1 to 1 kbp per second and τ_{res} is on the order of 20 to 30 min (22–24, 52, 53).

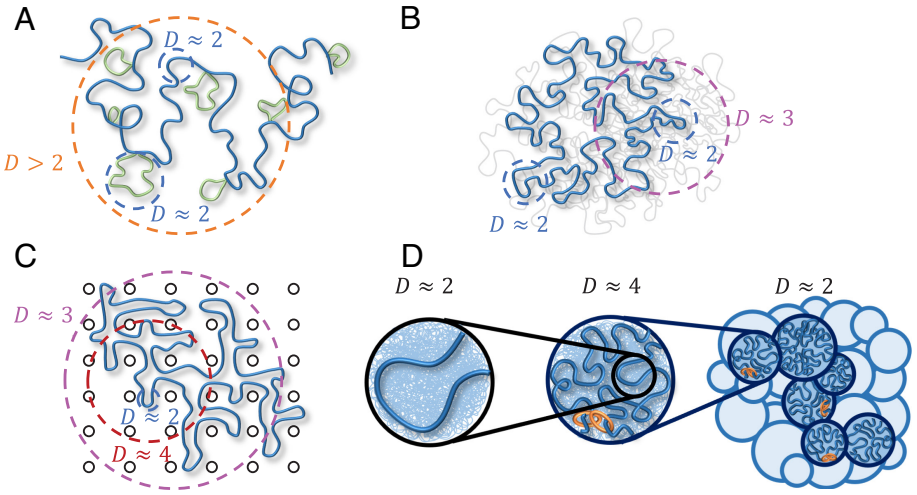

Fig. 3. Polymer models relevant to chromatin organization consistent with fractal dimension $D > 2$. Dashed circles indicate typical length scales with a given fractal dimension. (*A*) CPEL (44, 46). Looped and unlooped sections of the same polymer chain are drawn in green and blue, respectively. (*B*) FLG (47). Fractal behavior is shown for one polymer ring of interest (thick blue curve). Thin gray curves represent other polymers in a melt. (*C*) DFLA (48, 49). Fractal behavior is shown for one polymer ring of interest (thick blue curve). Black circles represent obstacles created by fixed networks. (*D*) Active loop extrusion (this paper). Short, relaxed sections of chromatin with fractal dimension $D \approx 2$ (*Left*) pack together to form extruded loops with $D \approx 4$ (center, where the most recently extruded section of a loop is shown in blue, the rest of the loop represented by the thin blue lines in the background, and orange rings represent cohesin). Extruded loops form a random walk (dark blue circles in the right-hand schematic) with $D \approx 2$ surrounded by other chromatin sections (light blue circles). Models (*A*–*C*) are equilibrium, while (*D*) is nonequilibrium.

In this work, we develop a scaling-level theory to describe chromatin organization due to active loop extrusion. We first describe the effect of active extrusion on relaxed chromatin with fractal dimension $D \approx 2$. We test the predictions of our model by hybrid molecular dynamics—Monte Carlo (MD—MC) simulations of a single extrusion cycle on relaxed polymer chains in a theta-like solvent. Next, we extend our model to chromatin conformation regulated by steady-state extrusion (in which cohesins randomly bind and unbind along the genome) with and without TAD anchors. We compare our model to simulations of steady-state extrusion on 1 Mbp chromatin sections in a theta-like solvent. We then discuss how active loop extrusion kinetically suppresses overlaps of neighboring sections of chromatin, dilutes entanglements, and segregates TADs. Our model also describes how extrusion deforms chromatin outside of growing loops and the spatial dynamics of actively extruding cohesins and chromatin loci. We compare our model to experimental data, finding consistency between our predicted contact probability scaling behavior and $P(s)$ from Micro-C (26, 32) as well as our predictions of chromatin locus dynamics and live-cell imaging experiments (54). This model explains the anomalous scaling exponent observed in contact probabilities $P(s) \sim s^{-0.75}$ and supports active loop extrusion as a mechanism for segregating TADs, thereby enhancing contacts between promoters and regulatory elements within the same TAD while suppressing off-target interactions.

Results

Model Description. Consider chromatin discretized into loci each with spatial size b and z base pairs (Fig. 4). If unperturbed (without loop extrusion), chromatin has fractal dimension $D = 2$ for genomic lengths longer than z: a section with genomic length s has mean square size

$$< r^2(s) > \approx b^2 \frac{s}{z}. \quad [1]$$

Throughout this work, $\approx$ indicates approximate equivalence within a factor on the order of unity and $\sim$ indicates proportionality. For definiteness we let each locus represent $z = 2$ kbp with $b \approx 50$ nm (see *SI Appendix* for estimate), assuming the persistence length of chromatin is of equal or smaller size. While the persistence length of chromatin is not known, the principles of our model still hold for different choices of persistence length and locus size. In the absence of active forces, loci follow Rouse-like dynamics on length scales smaller than entanglement length with mean square displacement (MSD)

$$MSD_{chr}(\Delta t) \approx b^2 \left(\frac{\Delta t}{\tau_0}\right)^{\frac{1}{2}} \text{for } \Delta t \geq \tau_0, \quad [2]$$

where Δt is the lag time and τ_0 is the locus diffusion time (34). The locus diffusion time is the time it takes a locus to move by thermal motion a distance on the order of its size. The relaxation time of a section with genomic length s and fractal dimension $D = 2$ is approximately

$$\tau_s \approx \tau_0 \left(\frac{s}{z}\right)^2, \quad [3]$$

which is the time it takes for the section with genomic length s to move by thermal motion a distance on the order of its unperturbed size (34).

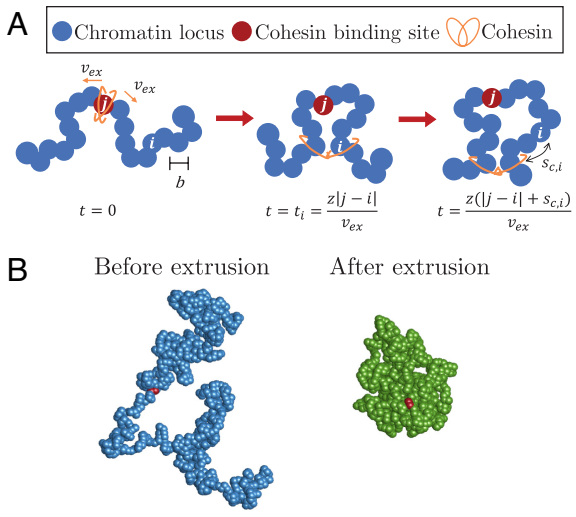

Fig. 4. Schematic of active loop extrusion model and simulation snapshots. (*A*) Chromatin is discretized into loci with size b each representing z base pairs. Cohesin domains bind to locus j and extrude away from one another with average curvilinear velocity v_{ex} in units of the number of base pairs per unit time. Locus i is extruded at the time $t_i = z|j-i|/v_{ex}$. At time $z\left(|j-i| + s_{c,i}\right)/v_{ex} > t_i$, locus i is $s_{c,i} = v_{ex}(t - t_i)$ base pairs away from the cohesin. (*B*) Snapshots of a hybrid MD—MC simulation of a single active loop extrusion cycle when a single cohesin extrudes a single bead-spring polymer chain once. The snapshots are before extrusion starts with $D \approx 2$ (*Left*, blue) and after the cohesin reaches the chain ends (*Right*, green). Each bead represents 1 kbp of chromatin (see *SI Appendix* for details). The red beads indicate the cohesin binding site.

We model cohesin as having two domains that bind to chromatin (Fig. 4). Domains extrude independently and in opposite directions along the chromatin contour with average curvilinear velocity v_{ex} in units of genomic length per unit time. The extrusion velocity v_{ex} and locus diffusion time τ_0 define a dimensionless parameter that we call the "extrusion ratio"

$$\kappa = v_{ex}\tau_0 z^{-1}, \quad [4]$$

which is the ratio of rates of active and passive dynamics for a locus of z base pairs, like a Péclet number describing the ratio between flow and diffusion effects on some length scale. The extrusion ratio is the number of loci extruded per diffusion time of a locus. The genomic length unimpededly extruded during time t is $v_{ex}t$. Since the two cohesin domains extrude independently, the average genomic length of the loop (loop length) at time t is

$$l \approx 2v_{ex}t = \frac{2\kappa z t}{\tau_0}, \quad [5]$$

and the cohesin processivity is $\lambda \approx 2v_{ex}\tau_{res} = 2\kappa z\tau_{res}/\tau_0$. Recall that cohesin processivity is defined as the average loop length extruded by unobstructed cohesin during the average residence time τ_{res} it is bound to chromatin. In our model, chromatin-bound cohesins have a probability of unbinding e^{-h} with attempt frequency τ_c^{-1} in units of reciprocal time. $h\ k_BT$ is an effective energy barrier for cohesin unbinding. Both the residence time and processivity are exponentially distributed with averages $\tau_{res} \approx \tau_c e^h$ and $\lambda \approx 2v_{ex}\tau_{res}$, respectively (see *SI Appendix* for more details). Although we choose this particular framework for cohesin binding, we expect the main results of our model to hold for other mechanisms.

Several experiments have observed chromatin loci with $MSD_{chr}(\Delta t) \approx D_{1/2}\Delta t^{1/2}$ consistent with Rouse-like dynamics where $D_{1/2}$ ranges between $\approx 10^{-3}$ $\mu m^2\ s^{-1/2}$ and $\approx 10^{-2}$ $\mu m^2\ s^{-1/2}$ (54–59). This coefficient is frequently called the "apparent diffusion constant" or "apparent diffusivity" D_{app}; however, since it does not have units of a true diffusion constant (length squared per time), we prefer to use D_α and call it the subdiffusive mobility coefficient, where α is the exponent describing the time dependence. For discretization of $z = 2$ kbp per locus each with size $b \approx 50$ nm and $v_{ex} \approx 0.1$ kbp per second, we estimate the extrusion ratio for cohesin (Eq. 4) to be on the order of $\kappa \approx 0.003 - 0.3$ (*SI Appendix*). Note that the wide range of observed $D_{1/2}$ causes a factor of 100 between the lower and upper estimates of the extrusion ratio. For definiteness, we use $\kappa \approx 0.2$ to make biological estimates throughout the paper and provide ranges of estimated parameters in *SI Appendix*, Table S2.

To test our theory, we use hybrid MD—MC simulations to model active loop extrusion on a single bead-spring polymer chain in a theta-like solvent with each bead representing 1 kbp and Kuhn length $\approx 2\sigma_{LJ}$, where σ_{LJ} is the bead diameter. See *Materials and Methods* and *SI Appendix* for details. Relaxed polymer conformations in theta-like solvents are random walks with $D \approx 2$ on scales longer than the Kuhn length, like dense solutions or melts of flexible linear polymers between the correlation and entanglement length scales, similar to conditions in the nucleus (34). We show results of three types of simulations in the main text: single active loop extrusion cycles where one cohesin extrudes an initially relaxed chain once (Fig. 4*B*); steady-state active loop extrusion where many cohesins bind, unbind, and extrude without TAD anchors; and steady-state active loop extrusion with TAD anchors.

Extrusion Forms Compact Chromatin Loops Composed of Overlapping Relaxed Sections. We start by describing the conformation of a single loop produced by active loop extrusion on a relaxed chromatin section with $D \approx 2$. The main concept of our model is that chromatin sections longer than genomic length $g_{min} \approx z/\kappa$ relax slower than the time it takes a single cohesin domain to extrude them. The relaxation time of a chromatin section with genomic length s is proportional to s^2, the square of its genomic length, while the time it takes to extrude it is proportional to s (Eqs. **3** and **5** and Fig. 5*A*). The asymptotic behavior of the mean square size of a loop with genomic length l is

$$< R^2(l) > \approx \begin{cases} b^2\frac{l}{2z}, & \frac{l}{2} \le g_{min} \\ b^2\left(g_{min}\frac{l}{2z^2}\right)^{\frac{1}{2}}, & g_{min} < \frac{l}{2} \end{cases}, \quad [6]$$

as plotted in Fig. 5*B*. This scaling behavior could be impacted by the spatial mobility of cohesins (*SI Appendix*). For a short loop with $l \le 2g_{min}$, the entire loop is relaxed (Eq. **1**). Longer loops cannot relax, so their sizes are determined by subdiffusive Rouse-like dynamics with $< R^2(l) > \sim t^{1/2} \sim l^{1/2}$. These loops are composed of multiple relaxed sections (Fig. 5*C*), the smallest with genomic length g_{min} and the largest with genomic length

$$g(l) \approx \left(\frac{lz}{2\kappa}\right)^{\frac{1}{2}} \approx \left(g_{min}\frac{l}{2}\right)^{\frac{1}{2}}, \quad [7]$$

and mean square size $\xi^2(l) \approx b^2\left[g_{min}l/\left(2z^2\right)\right]^{1/2}$ (see *SI Appendix* for details). For an extrusion ratio of $\kappa \approx 0.2$ and processivity $\lambda = l \approx 200$ kbp, the smallest relaxed chromatin section has genomic length $g_{min} \approx 10$ kbp and the largest has genomic length $g(\lambda) \approx 30$ kbp.

Consider $< r_l^2(s) >$, the mean square distance between any two loci separated by a genomic distance s extruded by the same cohesin domain in a loop with length l. The average is taken over all loci pairs separated by s within the loop. Like Eq. **6**, $< r_l^2(s) >$ crosses over between power laws $\sim s$ and $\sim s^{1/2}$ because short genomic sections are relaxed while long sections are not:

$$< r_l^2(s) > \approx \begin{cases} b^2\frac{s}{z}, & s \le g(l) \\ b^2\frac{[g(l)s]^{\frac{1}{2}}}{z}, & g(l) < s \end{cases}, \quad [8]$$

see Fig. 5*D*. The crossover between the two power laws occurs at genomic lengths on the order of $g(l)$ (Eq. **7**) because the largest relaxed sections with the largest number of loci pairs dominate the mean square distances averaged over all loop loci. Eq. **8** is consistent with a fractal dimension of $D \approx 4$ on genomic and spatial length scales longer than $g(l)$ and $\xi(l)$ respectively. Recall that within a mean-field approach, the contact probability function $P(s) \sim s^{-\gamma_i} \approx s^{-3/D_i}$ reflects the fractal behavior of the chromatin section of interest. Since compact loops transition between $D \approx 2$ and $D \approx 4$, the contact probability $P(s)$ within a single extruded loop is proportional to

$$P(s) \sim \begin{cases} s^{-\frac{3}{2}}, & s \le g(l) \\ s^{-\frac{3}{4}}, & g(l) < s \le \frac{l}{2} \end{cases}, \quad [9]$$

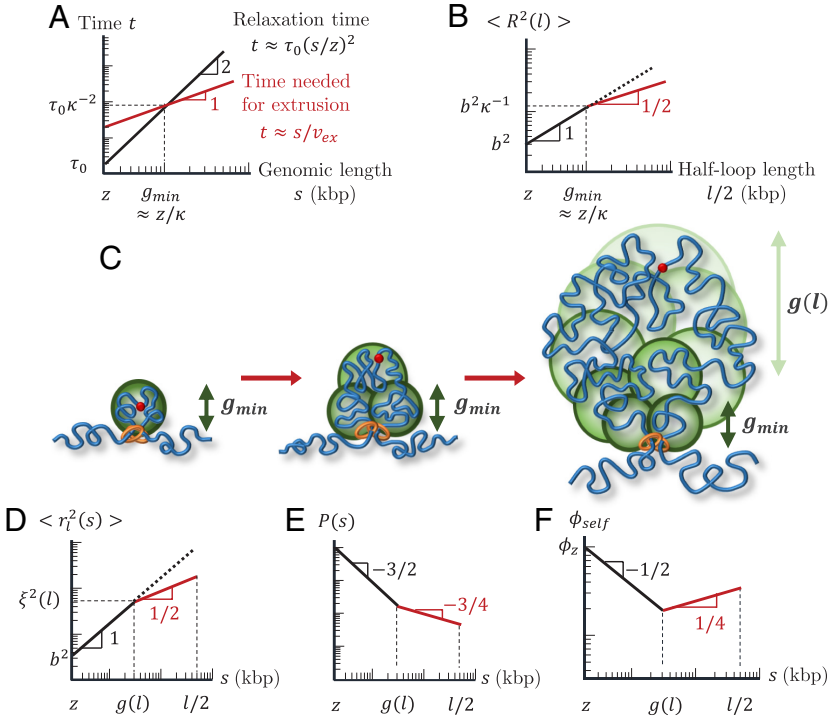

Fig. 5. Structure of an actively extruded loop. All schematic plots are on log–log scales. (*A*) Schematic plot comparing the relaxation time (black) and time needed for a single cohesin domain to extrude a chromatin section with genomic length s (red). (*B*) Schematic plot of the mean square size of a loop with genomic length l. The red line segment indicates the regime consistent with $D = 4$. The dotted line shows the mean square size of a chromatin section with genomic length $l/2$ without extrusion. (*C*) Relaxed sections (green circles) in a growing loop overlap in space forming a fractal with dimensionality $D = 4$. The smallest relaxed section has the genomic length $g_{min} \approx z/\kappa$. The genomic length of each relaxed section (green circles) grows from g_{min} next to the cohesin to $g(l) \approx (g_{min}l/2)^{1/2} \approx [lz/(2\kappa)]^{1/2}$ next to the cohesin binding site (red circle). (*D*) Mean square distance between two loci separated by a genomic distance s within a loop of genomic length l (Eq. **8**). The average is taken over all loci pairs within the loop extruded by the same cohesin domain. The red line segment indicates the regime consistent with $D = 4$. The dotted line shows the mean square distance without extrusion. (*E*) Average contact probability between loci separated by genomic length s within an extruded loop of length l. The red line segment indicates the regime consistent with $D = 4$. (*F*) Volume fraction ϕ_{self} of a chromatin section of length s within its own pervaded volume where the section is part of a loop with length l. The red line segment indicates the regime consistent with $D = 4$.

where $l/2$ is half of the loop length, after which contact probability increases (Fig. 5*E*). The results of simulations of a single cohesin extruding a loop on an initially relaxed chain are consistent with Eqs. **8** and **9** (Fig. 6).

How can chromatin loops have a fractal dimension of four in three-dimensional space? Analogous to randomly branched ideal polymers, the fractal dimension below spatial dimension 3 on small length scales creates enough space within a loop's pervaded volume for more compact structures with fractal dimension above 3 for a finite interval of larger length scales (34). Fig. 5*F* sketches the volume fraction ϕ_{self} for a section with genomic length s within its pervaded volume, where the section is part of a loop with genomic length l. We define volume fraction as the physical volume of chromatin (nucleosomes and linker DNA) of a genomic section with genomic length s divided by the approximately spherical volume spanned by the section (*SI Appendix*). Smaller loop sections with $s < g(l)$ are relaxed and therefore ideal with $D \approx 2$. The volume fraction ϕ_{self} within these small sections initially decreases with section genomic length s because the genomic length of a section grows slower than its pervaded volume $\sim s^{3/2}$. When $D \approx 4$, ϕ_{self} increases because the genomic length s and physical volume of the section grows faster than its pervaded volume $\sim s^{3/4}$. The volume fraction within a loop with genomic length l reaches $\phi_{self} \approx 2\phi_z\left[lz^2g(l)^{-3}/2\right]^{1/4}$. ϕ_z is the volume fraction of chromatin within one locus, which we estimate to be ≈0.1 for $z = 2$ kbp (*SI Appendix*). For $\kappa = 0.2$ and $z = 2$ kbp, ϕ_{self} within a loop with a typical genomic length $l \approx \lambda \approx 200$ kbp approaches ≈ 0.06, which is much smaller than unity. As such, a fractal dimension of four is possible for a wide range of genomic lengths.

Steady-State Active Loop Extrusion without TAD Anchors Compacts Chromatin on Scales Smaller than Processivity. We now consider many cohesins that actively extrude in a steady state with average processivity λ and separation d without including TAD anchors. Four regimes of processivity and separation dictate chromatin compaction and loop nesting on genomic length scales shorter than the genomic entanglement length with activity $N_{e,active}$ (see Fig. 7*A* and *SI Appendix* for details).

Fig. 7 *B*–*D* show schematic plots of contact probabilities $P(s)$ for each regime up to the entanglement genomic length. For all regimes, $P(s) \sim s^{-3/2}$ ($\gamma_1 \approx 3/2$) on short genomic length scales. In Regime I, the average processivity $\lambda \leq 2g_{min} \approx 2z/\kappa$ is small enough for entire loops to relax during their extrusion process. In Regime II, loops are long enough to be compact, but have time to fully relax before another cohesin binds with $d > \lambda(1 + 2\kappa\lambda/z)$. The system is heterogeneous with compact and relaxed sections; however, the average chromatin conformation is relaxed.

In Regime III, a loop extruded by cohesin only partially relaxes before another cohesin binds to this unrelaxed section with $\lambda(1 + 2\kappa\lambda/z) \geq d > \lambda$. In a steady state, cohesin separation controls the largest chromatin section that relaxes such that

$$g(d) \approx \left(\frac{dz^2}{2v_{ex}\tau_0}\right)^{\frac{1}{2}} \approx \left(g_{min}\frac{d}{2}\right)^{\frac{1}{2}}, \qquad [10]$$

where $d/(2v_{ex})$ is the average time between two cohesins binding within a chromatin section of length λ. $g(d)$ is the longest genomic length that relaxes between cohesin binding events in steady-state extrusion. Chromatin sections with shorter genomic lengths can fully relax before perturbation by another cohesin; chromatin sections with longer genomic lengths do not have enough time to relax. There is no loop nesting, but extrusion compacts the section from $D \approx 2$ to $D \approx 4$ such that $\gamma_2 \approx 3/4$ for $g(d) \leq s \leq C_1\lambda$, where C_1 is a constant on the order of unity. Extruding cohesins rarely simultaneously bind loci separated by much longer than λ; thus, for longer genomic lengths, chromatin is a random walk with $D \approx 2$ of compact, extruded sections each of which has $D \approx 4$ such that $\gamma_3 \approx 3/2$ (Fig. 2*B* and 6*B*).

In Regime IV, $\lambda \geq d$ indicates significant loop nesting and the genomic section compacts into a globule with almost constant $P(s)$ for $g(d) \leq s \leq C_1\lambda$. On longer genomic length scales, chromatin could either be a random walk of compact sections as in Regime III or elongate due to excluded volume interactions

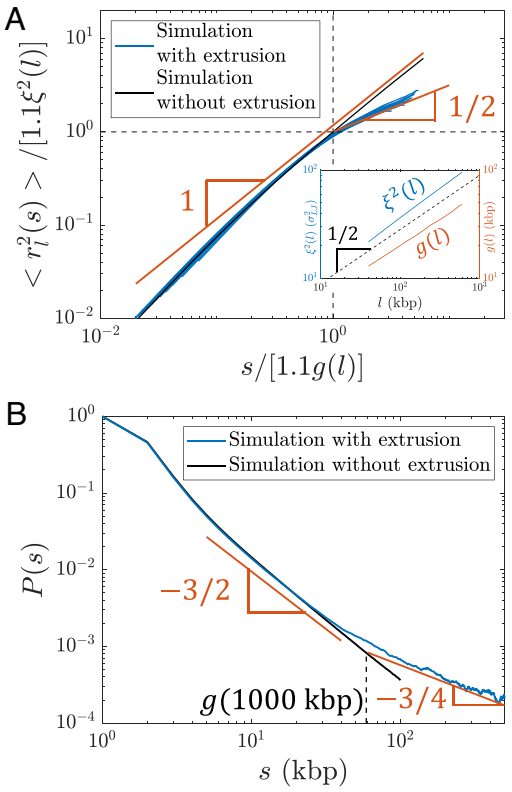

Fig. 6. Internal structure of actively extruded loops from hybrid MD—MC simulations with $v_{ex} \approx 0.6$ kbp per τ_0 ($\kappa \approx 0.3$) starting from a relaxed polymer chain with unperturbed fractal dimension $D \approx 2$. (*A*) Mean square distance between two loci extruded by the same cohesin domain separated by genomic distance s within a loop of genomic length l (Eq. **8**). Each blue curve corresponds to a different loop length l = 40, 80, 120, ..., 600 kbp. The red lines show the predicted scaling behavior. The abscissa and ordinate are scaled by $1.1g(l)$ and $1.1\xi^2(l)$, respectively. $g(l)$ and $\xi^2(l)$ were obtained from a simulation of relaxed chromatin without extrusion (see *Inset* and *SI Appendix* for details). The factor of 1.1 shifts the crossover between scaling behaviors to $s/[1.1g(l)] = 1$ and $< r_l^2(s) > / [1.1\xi^2(l)] = 1$ (dashed black lines). (*B*) Average contact probability between loci separated by genomic length s within an extruded loop, averaged over loop lengths $800 \le l \le 1{,}000$ kbp. The dashed vertical line indicates the crossover to $P(s) \sim s^{-3/4}$, which is approximately $g(1{,}000 \text{ kbp}) \approx 60$ kbp. The red lines show the predicted scaling behavior.

between compact sections, which depends on whether cohesins can traverse each other. This regime can produce bottlebrush-like structures relevant to mitotic chromosomes formed by condensins and will be explored in a future work.

There are too few cohesins per genomic length in Regimes I and II to compact chromatin. In Regime IV, chromatin adopts a nested structure that could form a bottlebrush not observed in interphase. Without entering the bottlebrush regime, chromatin compaction in Regime III is maximized when cohesin processivity and separation are approximately equal (by minimizing $g(d)$ in Eq. **10** and maintaining $\lambda \le d$). Indeed, cohesin processivity and separation in mammalian cells are both predicted to be on the order of 200 kbp with limited nesting (7, 11, 51). The remainder of this work focuses on Regime III.

TAD Anchors Can Limit the Range of Extrusion-Induced Compaction. Compaction can also be limited by TAD anchors; since CTCF stops active loop extrusion, cohesins cannot directly bridge two loci in different TADs separated by lengths much larger than average TAD genomic length $\overline{N_{TAD}}$ in the genomic section of interest. In this case, chromatin resembles a random walk of compact TADs with contact probabilities returning to $P(s) \sim s^{-3/2}$ for $C_2\overline{N_{TAD}} \le s < N_e$ where C_2 is a constant on the order of unity. We note that if the rate of cohesin binding within a TAD with genomic length comparable to λ is on the order of or greater than the rate of cohesins unbinding from TAD anchors, we predict the first crossover between $\gamma_1 \approx 3/2$ and $\gamma_2 \approx 3/4$ to remain at $s \approx g(d)$ (Eq. **10**).

We simulate steady-state active loop extrusion on a 1 Mega-base pair (Mbp) chromatin section with and without TAD anchors with $\lambda \approx d \approx 200$ kbp and $v_{ex} \approx 0.3$ kbp per τ_0 ($\kappa \approx 0.15$). CTCF sites were placed such that there were five consecutive TADs each with a genomic length of 200 kbp (Fig. 8*A*). The simulated $P(s)$ curves (Fig. 8*B*) are consistent with the expected scaling behavior depicted for Regime III in Fig. 7*C*. Without TADs, the crossover between $\gamma_2 \approx 3/4$ and $\gamma_3 \approx 3/2$ occurs at approximately $s \approx 400$ kbp, suggesting that the constant C_1 in Fig. 7*C* is approximately 2. With TAD anchors, the crossover occurs at the average TAD length $\overline{N_{TAD}} = 200$ kbp. The peaks at $s = 200$ kbp and $s = 400$ kbp are due to the periodicity introduced by consecutive TADs.

Experimental Data Are Consistent with the Predicted Contact Probability Scaling. Next, we compare our theory with publicly available Micro-C data. We expect $P(s)$ to follow Regime III in Fig. 7*C* with crossovers between $\gamma_1 \approx 3/2$ and $\gamma_2 \approx 3/4$ at $s \approx g(d)$ and between $\gamma_2 \approx 3/4$ and $\gamma_3 \approx 3/2$ at $s \approx C_2\overline{N_{TAD}}$. Recall that the first crossover is determined by the longest genomic section that can relax between cohesin binding events, which is related to separation d. As discussed in the "*Model Description*" and *SI Appendix*, we choose an extrusion ratio of $\kappa \approx 0.2$, indicating fast extrusion relative to chromatin relaxation within the range of observed chromatin loci mobilities. We reason that using genome-wide Micro-C data smooths out local variations in the lengths and genomic locations in TADs. To predict genome-wide $P(s)$ in mammalian cells, we use 30 kbp as the crossover location between γ_1 and γ_2 and 400 kbp as the crossover location between γ_2 and γ_3 (using $C_2 \approx C_1 = 2$). In Fig. 8*C* we plot this predicted $P(s)$ scaling (solid black lines) and two examples of genome-wide contact probabilities from Micro-C data in HFF and mESC [blue and green open circles, respectively (26, 32)]. We do not expect experimental Micro-C data to exactly follow the predicted asymptotic scaling; differences between single cells, genomic regions, and CTCF binding smooth the sharp transitions between regimes. Different experiments and cell types can also produce deviations between $P(s)$ curves, as seen by the difference between the HFF and mESC Micro-C data. Thus, we fit each Micro-C dataset to a crossover function between the three predicted power laws (blue and green solid curves, see *SI Appendix* for details). The crossover genomic lengths between scaling regimes for both HFF and mESC are close to our predicted values of 30 kbp and 400 kbp (*SI Appendix*, Table S4). We also fit the two Micro-C datasets simultaneously and achieve similar results (*SI Appendix*, Fig. S13). The error between the data, fits, and asymptotic scaling are smaller than the difference between the HFF and mESC datasets between 5 kbp and 1 Mbp, suggesting that our theory is consistent with $P(s)$ in these mammalian cells within experimental and cell type variation (*SI Appendix*, Table S4). We quantify error as the rmsd between the natural logarithms of two $P(s)$ curves. We note that the fits to individual Micro-C datasets perform better than both the simultaneous fit and the asymptotic scaling, indicating that the detailed shape of $P(s)$ depends on organism and cell type. Fig. 8*D* shows that the slopes on a log–log scale of the two experimental datasets are consistent with our model, suggesting that our choice of $\kappa \approx 0.2$ is reasonable. This scaling behavior is also consistent

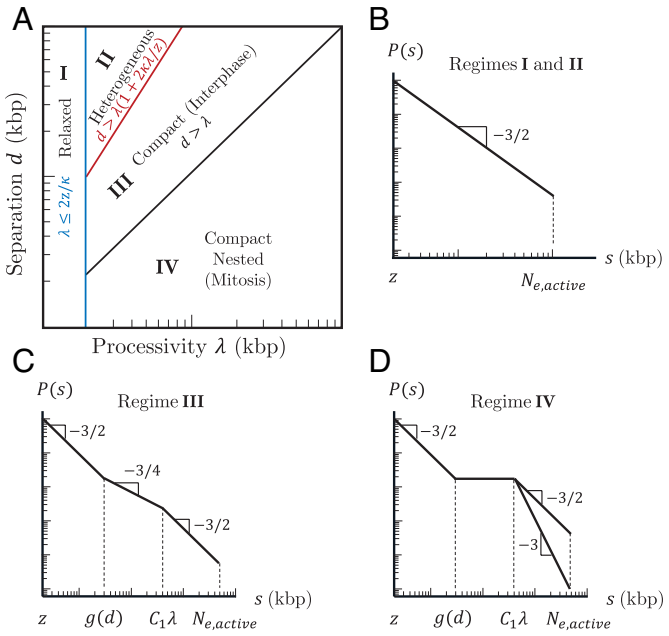

Fig. 7. Four regimes of chromatin compaction and nesting. (*A*) Diagram indicating the four regimes of chromatin compaction and nesting as functions of cohesin processivity and separation. (*B–D*) Schematic contact probabilities on log–log scales for the different regimes. In (*D*), genomic separations of $C_1\lambda < s \leq N_{e,active}$ may have $P(s) \sim s^{-3/2}$ or $P(s) \sim s^{-3}$ depending on whether cohesins can traverse each other.

with other Hi-C and Micro-C experiments (5, 8, 25–27, 29–32). We note that specific genomic sections may have different average TAD lengths $\overline{N_{TAD}}$, which could shift the crossover between γ_2 and γ_3.

Active Loop Extrusion Kinetically Suppresses Overlaps and Dilutes Entanglements. Another consequence of chromatin compaction due to active extrusion is the reduction of overlap between neighboring chromatin sections and entanglement dilution. We define the overlap parameter $O(s)$ as the number of chromatin sections with genomic length s with the same mean square spatial size $< r^2(s) >$ that share the same approximately spherical volume with diameter $\approx < r^2(s) >^{1/2}$

$$O(s) \approx \phi \frac{\pi z}{6sv} < r^2(s) >^{\frac{3}{2}}, \qquad [11]$$

where $\phi \approx 0.06 - 0.4$ is the average chromatin volume fraction in the nucleus and v is the physical volume occupied by a locus, which for $z \approx 2$ kbp we estimate to be $\approx 7.5\text{x}10^3$ nm^3 (*SI Appendix*). If a chromatin section with genomic length s has a fractal dimension of D between length scales b and $< r^2(s) >^{1/2}$, the overlap parameter is $O(s) \approx \left[\pi b^3/(6v)\right]\phi(s/z)^{3/D-1}$. Entanglements occur above a critical overlap parameter O_{KN} on the order of 10 to 20 as conjectured by Kavassalis and Noolandi (60). If chromatin has $D \approx 2$ without loop extrusion, the entanglement genomic length is approximately $N_{e,passive} \approx 100$ kbp for an average chromatin volume fraction $\phi \approx 0.15$ and $O_{KN} = 10$. Previous estimates suggest an entanglement genomic length without extrusion nor extensive looping of 50 to 100 kbp (33, 42–44). Our estimate of $N_{e,passive} \approx 100$ kbp is also consistent with Hi-C data showing a contact probability scaling of $P(s) \sim s^{-0.94}$ for 100 kbp $< s <$ 500 kbp in cohesin-depleted cells (25).

With active loop extrusion, the overlap parameter decreases with genomic length when $D \approx 4$, which we predict to occur on genomic length scales between $\approx g(d)$ and $\approx 2\overline{N_{TAD}}$ (Fig. 9). The mean square size of genomic sections longer than $g(d)$ is smaller with active loop extrusion compared to the passive case with random walk statistics up to entanglements. As such, longer genomic sections are required to reach O_{KN} such that

$$N_{e,active} \approx N_{e,passive} \left[\frac{2\overline{N_{TAD}}}{g(d)}\right]^{\frac{3}{2}}. \qquad [12]$$

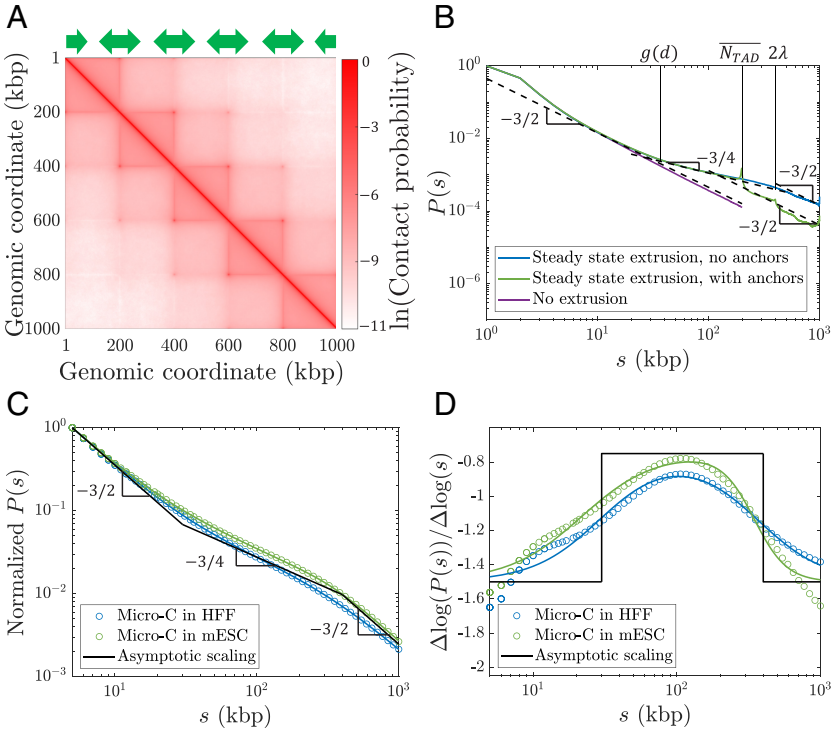

Fig. 8. Contact probabilities from simulations with steady-state extrusion and public Micro-C data. (*A*) Contact map from a simulation with 1,000 kbp. CTCF sites were placed according to the green arrows such that there were five consecutive TADs of 200 kbp each. (*B*) Contact probabilities from simulations with and without TADs. Dashed black lines show power laws $P(s) \sim s^{-3/2}$ and $P(s) \sim s^{-3/4}$. (*C*) Genome-averaged contact probabilities normalized to $P(5\text{ kbp}) = 1$ from Micro-C in HFF [blue open circles, (26)] and mESC [green open circles, (32)] at 1 kbp resolution compared to theoretically expected scaling behavior (solid black lines) and independent fits to a crossover function (blue and green solid curves, see *SI Appendix*, Eq. **S38**). Fractal dimension is predicted to cross-over from 2 to 4 at 30 kbp, and back to 2 at 400 kbp as shown by the solid black lines. (*D*) Slopes on a log–log scale of curves in (*C*).

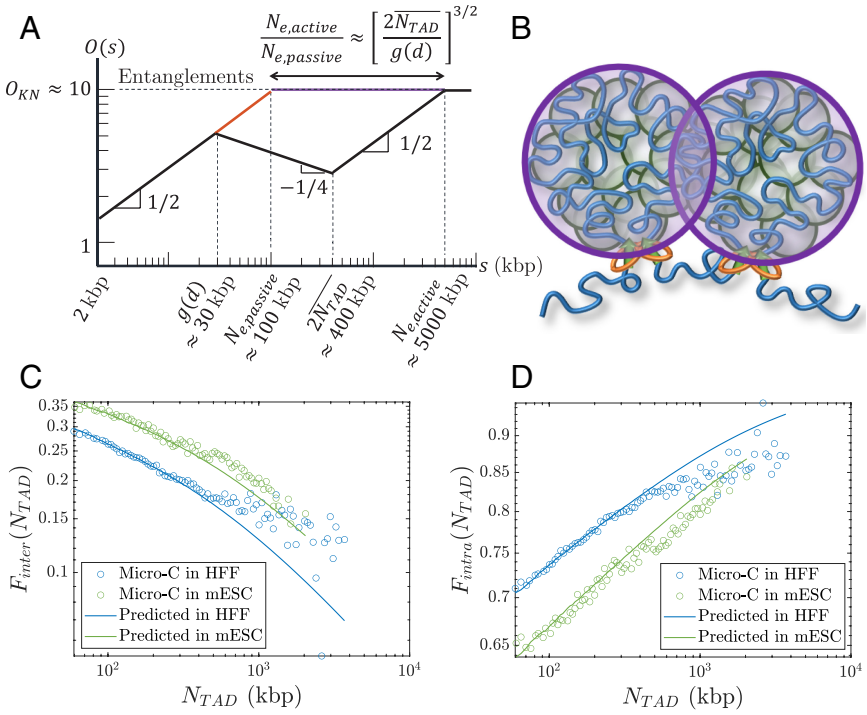

Fig. 9. Overlaps between chromatin sections. (*A*) Schematic plot of the overlap parameter $O(s)$ for active loop extrusion (black), random walks (red), and FLGs (purple) as a function of genomic length on a log–log scale. The black and purple curves merge for $s \geq N_{e,active}$. The horizontal dashed line indicates the onset of entanglements. We use the volume fraction of chromatin in the nucleus $\phi = 0.15$ and $O_{KN} = 10$. (*B*) Chromatin sections within TADs (green circles) overlap and have increased contact probabilities. Neighboring TADs (purple circles) are mostly segregated apart from a narrow interface. (*C*) Inter-TAD fraction of all intrachromosomal contacts made by loci in a TAD as a function of TAD length. (*D*) Intra-TAD fraction of all intrachromosomal contacts made by loci in a TAD as a function of TAD length.

With $2\overline{N_{TAD}} = 400$ kbp and $g(d) = 30$ kbp, active loop extrusion can increase N_e by up to a factor of approximately 50. If the passive entanglement genomic length is 50 to 100 kbp, active loop extrusion could dilute entanglements up to genomic lengths of 2.5 to 5 Mbp. In *SI Appendix*, Table S3 we provide ranges for the entanglement genomic lengths for different chromatin volume fractions ϕ and O_{KN}.

Active Loop Extrusion Segregates TADs and Enhances Intra-TAD Contacts. The increase in fractal dimension to $D \approx 4$ due to active loop extrusion is consistent with TAD segregation. Loop extrusion decreases TAD overlap compared to random walks with $D \approx 2$ and FLGs with $D \approx 3$. In the FLG model, the overlap parameter remains constant at $O_{KN} \approx 10$ above the entanglement genomic length, which with $N_{e,passive} \approx 50 - 100$ kbp indicates relatively strong overlap of genomic loci between TADs. If this were the case, regulatory elements would frequently affect promoters in different TADs. On the other hand, the decrease in overlap parameter with active loop extrusion by a factor of $\left[s/g(d)\right]^{3/2}$ for $g(d) \leq s \leq 2\overline{N_{TAD}}$ (Fig. 9) indicates that genomic contacts between TADs are suppressed compared to contacts within TADs. Active loop extrusion suppresses the number of overlapping TADs compared to the passive case (without extrusion) by up to a factor of $\approx \left[2\overline{N_{TAD}}/g(d)\right]^{3/4}$. For $2\overline{N_{TAD}} = 400$ kbp and $g(d) = 30$ kbp, this reduction factor is approximately 7. For $\phi = 0.15$ and $O_{KN} = 10$, the overlap parameter at 400 kbp reduces from ≈ 16 to ≈ 3. Note that because our theory is on a scaling level and the degree of overlap between genomic sections depends on the shape of their pervaded volumes (e.g., spherical, or ellipsoidal), our estimates can differ from real biological systems by a factor of two.

Our model suggests that while contacts between TADs are suppressed, contacts between sections within the same TAD are enhanced. Loci in each TAD mostly contact other loci separated by less than 400 kbp within the same TAD, apart from a narrow zone of interaction at the interface between neighboring TADs (Fig. 9*B*). Future simulations will further investigate this effect. Analysis of Micro-C data shows that out of all intrachromosomal contacts made by loci in a TAD of length N_{TAD}, the inter-TAD fraction $F_{inter}(N_{TAD})$ (contacts between loci in the TAD and other loci on the same chromosome but not in the same TAD) is $\lesssim 0.35$ and monotonically decreases with TAD length (Fig. 9*C*). Conversely, the intra-TAD fraction $F_{intra}(N_{TAD})$ (contacts between loci in the TAD and other loci within the same TAD) is $\gtrsim 0.65$ and monotonically increases with TAD length (Fig. 9*D*). Predictions using our theory agree with Micro-C data in HFF and mESC (Fig. 9 *C* and *D*). See *SI Appendix* for details. As such, active loop extrusion facilitates colocalization of promoters and regulatory elements within the same TAD while limiting erroneous contacts between TADs.

Active Loop Extrusion Extends Chromatin Adjacent to Loops. Cohesin pulls on chromatin directly adjacent to loops, causing two tension fronts that propagate into the unextruded sections (Fig. 10*A*). We use the term "leg" to denote the largest chromatin section that adapts to this pulling force. Active extrusion suppresses the relaxation modes of the legs, as cohesin translocation is ballistic. Cohesin translocation rather than polymer relaxation controls leg conformation. Cohesin reels in chromatin legs, each with genomic length $g_{leg}(t)$, and unravels their conformations. Loci separated by more than $g_{leg}(t)$ past cohesin are not "aware" of extrusion. The mean square size of a leg $< r^2_{leg}(t) >$ is approximately the mean square size of a genomic length $v_{ex}t + g_{leg}(t)$ before extrusion started such that $< r^2_{leg}(t) > \sim \left[v_{ex}t + g_{leg}(t)\right]^{2/D} \approx \left(v_{ex}t\right)^{2/D}$ with corrections due to partial relaxation. Each leg is extended such that its genomic length is $g_{leg}(t) \sim < r^2_{leg}(t) >^{1/2} b^{-1} \sim \left(v_{ex}t\right)^{1/D}$ (*SI Appendix*).

Consider $< r^2_{coh}\left(s_{c,out}\right) >$, the mean square distance between cohesin and a locus $s_{c,out}$ base pairs outside of the loop. The limiting behavior is a straight array of loci with $< r^2_{coh}\left(s_{c,out}\right) > \approx \left(bs_{c,out}/z\right)^2$. For genomic distances longer than the leg length, $< r^2_{coh}\left(s_{c,out}\right) >$ is approximately equal to $< r^2_0\left(s_{c,out} + v_{ex}t\right) >$, the mean square distance between the cohesin binding site and the locus of interest before extrusion

started. Hybrid MD—MC simulations of a single cohesin extruding a loop on an initially relaxed polymer chain are consistent with this result (Fig. 10*B*).

Active Loop Extrusion Causes Anomalous Dynamics of Actively Extruding Cohesins and Chromatin Loci. The two tension fronts (one tension front produced per leg) localize an actively extruding cohesin in the volume between them. A cohesin's trajectory follows the midpoint between the two tension fronts (Fig. 11*A*) and fluctuates around it by $\approx b^2\left(t/\tau_0\right)^{1/2}$. Hybrid MD—MC simulations agree with this result (Fig. 11*B* and *SI Appendix*, Fig. S6). Multiple unnested cohesins attract each other in space because they exert tension on the same intervening genomic sections. After the cohesins meet, they travel together in space; this effect is more pronounced if the cohesins cannot traverse one another (*SI Appendix*). This "self-focusing" effect of neighboring cohesins further maintains the compact structure of actively extruded chromatin. Future work will explore additional details, including the nested cohesin case.

The MSD of cohesin $MSD_{coh}(\Delta t)$ is coupled on short time scales to the Rouse modes of the smallest relaxed chromatin section g_{min} and is proportional to $\Delta t^{1/2}$ for lag times $\Delta t \leq \Delta t^{+}_{coh} \approx \tau_0 \kappa^{-2}$. Cohesin trajectories then follow tension fronts dictated by the chromatin conformation such that $MSD_{coh} \sim \Delta t^{2/D}$. Upon steady-state extrusion, the cohesin MSD for $\Delta t \geq \Delta t^{+}_{coh}$ crosses over between scaling behaviors of $\sim \Delta t$ and $\sim \Delta t^{1/2}$ at $\Delta t^{++}_{coh} \approx g(d)/v_{ex}$ (Fig. 11*C* and *SI Appendix*, Fig. S7). Δt^{++}_{coh} is approximately the time it takes a cohesin domain to extrude a genomic length $g(d)$ in the process of active loop extrusion. Both crossover times Δt^{+}_{coh} and Δt^{++}_{coh} depend on the $D_{1/2}$ of the chromatin section of interest, where the chromatin locus MSD is $MSD_{chr}(\Delta t) \approx D_{1/2}\Delta t^{1/2}$ (*SI Appendix*). For $\kappa \approx 0.2$, a locus discretization of $z = 2$ kbp per locus, and locus size $b = 50$ nm, we predict Δt^{+}_{coh} to be on the order of 100 s and $\Delta t_{coh}{}^{++}$ to be on the order of 300 s.

In the Rouse model of polymer dynamics, the MSD of monomers in a polymer with fractal dimension D scales as $\sim \Delta t^{2/(D+2)}$ (34). The change in chromatin fractal dimension due to active loop extrusion on scales below cohesin processivity causes $MSD_{chr}(\Delta t)$ to cross-over between scaling behaviors of $\sim \Delta t^{1/2}$ and $\sim \Delta t^{1/3}$ (Fig. 11*D* and *SI Appendix*, Fig. S8). The crossover time between regimes is $\Delta t^{+}_{chr} \approx d/\left(2v_{ex}\right) \approx \tau_0 d/(2z\kappa)$ (*SI Appendix*). In the absence of other activity, we predict the crossover to occur at lag times on the order of tens of minutes corresponding to $\Delta t^{+}_{chr} \approx 250\tau_0$. In *SI Appendix*, we discuss the MSD of chromatin loci for longer lag times. Experimentally, the two-point MSD (2pMSD) between the relative position of two loci is often measured rather than the MSD of a single locus (54, 62–64). The 2pMSD initially scales the same way as the single locus MSD with approximately twice the magnitude before it plateaus at twice the mean square distance between the two loci.

In Fig. 11*E*, we fit 2pMSD live-cell imaging data in mESC (54) to the predicted scaling behavior for lag times shorter than 6×10^3 s (*SI Appendix*). The green curve represents 2pMSD between two convergent CTCF sites in wild-type cells while the yellow curve is from cells in which the CTCF binding motifs were deleted (ΔCTCFsites). Our scaling prediction is consistent with the experimental data, though we note that the experimental 2pMSD could be approaching the characteristic plateau. The 2pMSDs at the fitted crossovers (dashed green and yellow lines in Fig. 11*E*) are close to our estimated value of $\approx 0.08\ \mu m^2$ (*SI Appendix*). For wild-type cells, the fitted subdiffusive mobility coefficient $D_{1/2} \approx 2.3 \times 10^{-3}\ \mu m^2\ s^{-0.5}$ means the crossover occurs at $\Delta t^{+}_{chr} \approx 200\tau_0$, which is consistent with our prediction (*SI Appendix*). With $d \approx 200$ kbp, this translates to reasonable values of extrusion velocity $v_{ex} \approx 0.5$ kbp/s, extrusion ratio $\kappa \approx 0.3$, and $g(d) \approx 26$ kbp (Eq. **10** and *SI Appendix*). This $g(d) \approx 26$ kbp obtained from 2pMSD data is the same as the crossover genomic length between $\gamma_1 \approx 1.5$ and $\gamma_2 \approx 0.75$ scaling exponents obtained from simultaneously fitting HFF and mESC Micro-C $P(s)$ (*SI Appendix*, Table S4) and similar to our predicted 30 kbp. Note that although specific interactions between CTCF sites could cause additional correlations in the 2pMSD that may need to be carefully considered, the predicted scaling is consistent with both the data with CTCF sites deleted and wild-type cells with CTCF sites intact. Future work could explicitly include interactions between genomic loci (whether they are convergent CTCF sites or a promoter–enhancer pair) to more accurately model experimental data.

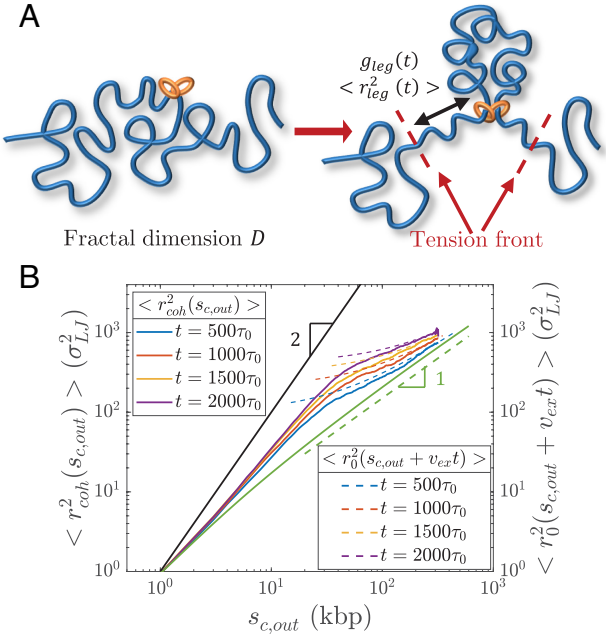

Fig. 10. Conformation of legs produced by active loop extrusion. (*A*) Schematic of legs, each with genomic length $g_{leg}(t) \sim (v_{ex}t)^{1/D}$ and mean square size $< r^2_{leg}(t) > \sim (v_{ex}t)^{2/D}$. The left-hand schematic shows the initial chromatin conformation with fractal dimension D at the time of cohesin binding. The right-hand schematic shows leg extension at time t. (*B*) Mean square distance between cohesin and a locus $s_{c,out}$ away outside of its extruded loop at different times after binding (solid lines) compared to $< r^2_0\ (s_{c,out} + v_{ex}t\ ) >$, the unperturbed mean squared sizes of sections with genomic lengths $s_{c,out} + v_{ex}t$ (dashed lines), from hybrid MD—MC simulations of single cohesins actively extruding a relaxed polymer chain ($D \approx 2$) with $v_{ex} \approx 0.3$ kbp per τ_0 ($\kappa \approx 0.15$). The solid black line is the predicted limiting behavior for full polymer extension. The solid green curve is the unperturbed mean square sizes of sections with genomic length $s_{c,out}$. The dashed green line is the predicted scaling behavior of these unperturbed sizes without extrusion.

Discussion

Summary. We present a theory and accompanying hybrid MD—MC simulations of chromatin organization and dynamics during interphase driven by active loop extrusion. Extrusion produces compact loops composed of overlapping relaxed chromatin sections (Fig. 5). We show that within extruded loops, chromatin conformation can have the fractal dimension of two on length scales smaller than the sizes of these relaxed sections. The loops are much more compact with fractal dimensions of four on larger length scales, with the crossover between these regimes at

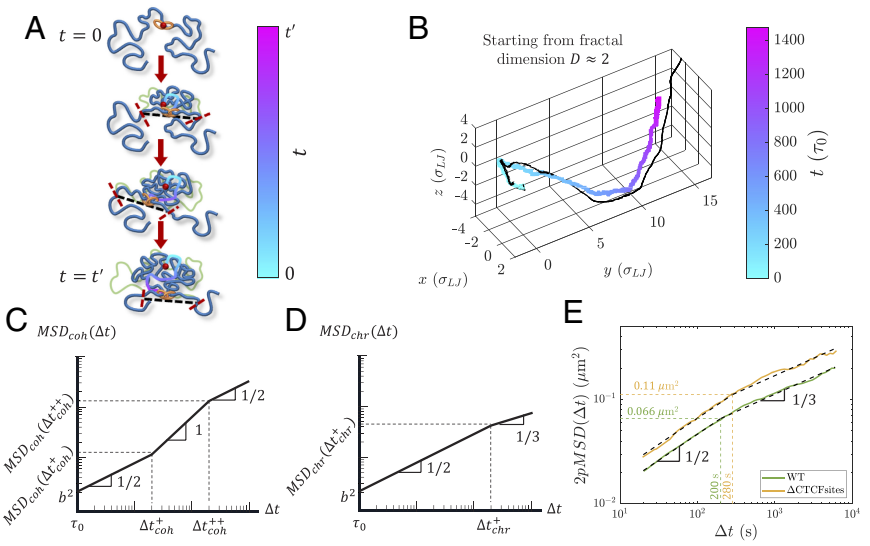

Fig. 11. Dynamics of cohesin and chromatin loci during active extrusion. (*A*) Cohesin trajectory (gradient curve) after binding to chromatin at its binding site (red circle) at time $t = 0$. The thick blue curve represents chromatin at a given moment, and the thin green curve represents the initial conformation. The gradient from cyan to magenta indicates time. Dashed black lines connect the tension fronts (indicated by dashed red lines) at different times, which propagate through the section with time. (*B*) Average cohesin trajectory (gradient curve) from a fixed binding site and the corresponding smoothed trajectory of midpoints between two tension fronts (black curve) from 200 simulations starting from the same initial conformations with $v_{ex} \approx 0.3$ kbp per τ_0 ($\kappa \approx 0.15$) starting from $D \approx 2$. (*C*) MSD of actively extruding, chromatin-bound cohesins on a log–log scale. (*D*) MSD of chromatin loci affected by active extrusion on a log–log scale. (*E*) 2pMSD between CTCF sites separated by 515 kbp in wild-type mESC (solid green curve) and cells with the CTCF binding motifs deleted (ΔCTCFsites, solid yellow curve) (54) fitted to the two power laws $\sim \Delta t^{1/2}$ and $\sim \Delta t^{1/3}$ (dashed black lines) predicted for genomic locus dynamics (see *SI Appendix* for fitting details). 2pMSD data were extracted using a plot digitizer (61). The dashed green and yellow lines indicate the intersection of the fitted power laws for wild-type and Δ CTCFsites cells, respectively.

chromatin strands of ≈30 kbp. We suggest that conformations of chromatin strands longer than TADs are random walks of looped sections with topological interactions appearing on scales of several Mbps. The predicted contact probability scaling behavior is consistent with publicly available experimental data (Fig. 8 *C* and *D*). Our model suggests that active loop extrusion increases the entanglement genomic length of chromatin by almost two orders of magnitude and segregates TADs (Fig. 9). We also predict the MSD for both actively extruding chromatin-bound cohesins (Fig. 11*C*) and chromatin loci (Fig. 11*D*). This work provides a theoretical explanation for the compact, largely unentangled structure of chromatin during interphase.

Active Loop Extrusion Is an Effective Mechanism for Transcriptional Regulation. Contacts between loci that may be separated by hundreds of kbp can up- or down-regulate genes (1). Active loop extrusion is an effective way of bringing genomic loci within physical proximity and segregating TADs, which may contribute to their insulating properties, consistent with TAD segregation observed with microscopy (39–41). At genomic separations of ≈ 400 kbp, active loop extrusion increases contact probabilities by factors of approximately 7 and 3 compared to random walks and FLGs, respectively. This model ensures that *cis*-regulatory elements mostly encounter promoters within the same TAD separated by up to 400 kbp due to the local minimum of overlap parameter on the order of unity at this scale (Fig. 9). Another consequence of chromatin compaction is the facilitation of transcription factor binding to chromatin (TF binding) within TADs. Active loop extrusion increases the volume fraction of a TAD within its pervaded volume. While a TF explores this volume, the frequency of encounters with its binding sites in the TAD increases. This is consistent with experimental evidence that cohesin depletion can impair TF binding, particularly for inducible TFs like the glucocorticoid receptor (65), by reducing the TF target search efficiency (32).

Cohesin Affects Large-Scale Chromatin Organization and Dilutes Entanglements. Cohesin-mediated chromatin compaction on scales shorter than 400 kbp reduces spatial overlaps between genomic sections, thus suppressing genomic entanglements (Fig. 9*A*). We predict the entanglement genomic length of chromatin with active loop extrusion to be approximately 5 Mbp. Our model is consistent with experiments showing that interphase chromatin is largely unentangled (45). Furthermore, recent work observed more disordered chromatin organization and anomalous genomic contacts on genomic length scales of several Mbps upon cohesin degradation (66), indicating that cohesin regulates chromatin conformation in a wide range of genomic lengths.

TAD Anchors Can Limit Chromatin Compaction. As seen in our computer simulations, TAD anchors can control the crossover between contact probability scaling exponents $\gamma_2 \approx 3/4$ and $\gamma_3 \approx 3/2$. Thus, the $P(s)$ profile can vary for genomic sections with different distributions of TADs. If the average TAD length $\overline{N_{TAD}}$ is greater than λ, we expect a negligible impact on $P(s)$ compared to without TAD anchors (i.e., Fig. 7*C* and the blue curve in Fig. 8*B*). Consecutive TADs each with length $\overline{N_{TAD}} < 2\lambda$ truncate the regime associated with γ_2 such that the crossover to γ_3 shifts to $\overline{N_{TAD}}$ (Fig. 8*B*). If $\overline{N_{TAD}}$ is shorter than both the cohesin processivity and separation, the location of the first crossover between $\gamma_1 \approx 3/2$ and $\gamma_2 \approx 3/4$ can also shift to $g\left(\overline{N_{TAD}}\right)$ (Eq. 7). This crossover could be impacted by how long TAD anchors are held together by cohesins compared to the average residence time of unimpeded cohesin. Consider two TAD anchors held together by a cohesin separated by a genomic length shorter than $\lambda \approx d$. Assume that other cohesins do not bind within the TAD while the anchors are held together. The longest genomic length that can relax is now determined by how long the anchors are held together. If the interaction between cohesin and CTCF stabilizes cohesin and increases its residence time, the crossover between $\gamma_1 \approx 3/2$ and $\gamma_2 \approx 3/4$ will shift to a longer genomic length.

Active Loop Extrusion Parameters Control Contact Probabilities. Extrusion velocity, cohesin processivity, and cohesin separation modulate contact probabilities both within loops formed by single cohesins and within sections regulated by multiple cohesins. In both cases, the first crossover in $P(s)$ between $\gamma_1 \approx 3/2$ and $\gamma_2 \approx 3/4$ can be tuned by extrusion velocity (Eq. **10**). Faster extrusion decreases the genomic length of chromatin sections that can relax, which increases compaction within each loop. When multiple cohesins organize a genomic section, decreasing the average cohesin separation can also shift this crossover to shorter genomic length scales (Eq. **10**), ideally by increasing cohesin binding frequency. More frequent cohesin binding results in shorter chromatin sections that relax between binding events. Cohesin processivity controls the crossover in $P(s)$ between $\gamma_2 \approx 3/4$ and $\gamma_3 \approx 3/2$ (as well as TAD anchors, as discussed above). Longer processivities (achieved, for example, by extending

cohesin residence times) increase the genomic separation between loci that can be held together by active extrusion. If experiments could develop fine control over the parameters of active loop extrusion in particular TADs, this work could help tune the contact probabilities between specific loci of interest.

Suggestions for Experimental Validation. As discussed in the previous paragraph, fine control over cohesin properties is ideal for changing contact probability curves in our model. A global decrease in cohesin binding frequency [perhaps by knocking down SCC4 (52, 67)] should extend the initial regime of $\gamma_1 \approx 3/2$ in genome-averaged contact probabilities and shorten the regime of $\gamma_2 \approx 3/4$, assuming extrusion velocity, cohesin processivity, and chromatin loci dynamics remain unchanged. Increasing cohesin residence times and processivities should extend the regime of $\gamma_2 \approx 3/4$; indeed, this "shoulder" in $P(s)$ associated with $\gamma_2 \approx 3/4$ qualitatively persists for longer genomic lengths in WAPL knockdown cells compared to wild-type (67, 68). In both the SCC4 and WAPL knockdown cases, cohesin properties should be characterized to determine which model parameters are modulated. Another way to tune the extent of the compact regime with $\gamma_2 \approx 3/4$ is to edit CTCF binding sequences within a specific genomic section such that there are consecutive "TADs." Changing the genomic length of the engineered TADs should control the crossover between γ_2 and γ_3 for contact probabilities within that specific genomic section.

To validate our model's predictions of chromatin locus MSDs (crossover between scaling behaviors of $\sim \Delta t^{1/2}$ and $\sim \Delta t^{1/3}$), we suggest live-cell imaging to obtain two-point MSDs between genomic loci similar to the work in refs. 54 and 62, which were done in mESC and *Drosophila melanogaster* embryos, respectively. We suggest additional experiments in mammalian cells, in which there is more evidence that active loop extrusion is important in shaping the genome than in *Drosophila* embryos (69). The two loci should be separated by at least 1 Mbp to reduce the effect of the two-point MSD plateau that limits the measured two-point MSD by the mean square distance between the two loci. We also suggest to choose two loci that do not interact via a known *cis*-regulatory interaction and that they are not convergent CTCF sites of a TAD. These explicit interactions could cause additional correlations between the two loci that may require careful analysis. We note that despite these potential limitations, the two-point MSDs in ref. 54 is consistent with a crossover between $\sim \Delta t^{1/2}$ and $\sim \Delta t^{1/3}$ (Fig. 11*E*).

Model Assumptions. One assumption of our model is that active loop extrusion is the main regulatory mechanism of chromatin organization. Recent studies have carefully examined the role of RNAPII in shaping chromatin organization, showing that specific chromatin loops and genomic sections are impacted by active transcription (27, 70–72). However, RNAPII degradation does not affect genome-wide contact probabilities $P(s)$ on genomic length scales shorter than 10 Mbp (27, 71). Furthermore, transcription is known to occur through bursting kinetics, with inactive periods on the order of hours (18, 73, 74). As a result, although transcription and other processes may affect chromatin organization at specific genomic locations, we reason that on average, genome organization is predominantly shaped by cohesin-mediated active loop extrusion.

We also assume that the crossovers between scaling regimes in $P(s)$ and overlap parameter $O(s)$ are well characterized by the average cohesin processivity and separation. The averages and distributions of these parameters could vary with genomic context, which could shift the crossover locations to different genomic length scales. Our computer simulations suggest that $P(s)$ averaged over a 1 Mbp section is well described by the average λ and d. More detailed simulations will confirm whether this is true for $O(s)$ as well. The crossover genomic lengths should not impact the asymptotic scaling behaviors of both $P(s)$ and $O(s)$ (ex., the γ_i exponents). Additionally, we assume that almost all contacts made by a given locus are intrachromosomal. Some process(es) must ensure that chromosomes are confined to localized volumes since it is well known that chromosomes segregate into territories (75). We leave the investigation of the phenomena that could lead to such segregation as an open question for future work.

Comparison with Other Models. As shown in Fig. 3, the CPEL, FLG, and DFLA models for chromatin organization are also consistent with fractal dimensions $D > 2$ (44, 46–49). In contrast to these three equilibrium models, we directly couple active, ATP-dependent extrusion kinetics to chromatin conformation and dynamics. The fractal dimension $D \approx 4$ between the scales of approximately 30 kbp and 400 kbp is a direct result of activity. With respect to CPEL, the looped sections with $D \approx 2$ could be interpreted as analogous to relaxed sections with genomic length $g(d)$ in our model. However, in CPEL the relaxed loop lengths are exponentially distributed, whereas in our model, the extruded loop lengths are exponentially distributed while the relaxed sections within an extruded loop are uniformly distributed (*SI Appendix*). In contrast to FLG, our model explains the anomalous fractal dimension of $D \approx 4$. We suggest that chromatin sections longer than $N_{e,active}$ maintain constant overlap like in FLG (Fig. 9). Finally, to compare with DFLA, the polymer sections between fixed obstacles with $D \approx 2$ may be analogous to the relaxed sections with genomic length $g(d)$ in our model.

Conclusion

In conclusion, our model explains how active loop extrusion compacts individual chromatin loops, forms segregated TADs, and dilutes chromatin entanglements. This work suggests a crucial role of loop-extruding proteins in maintaining effective regulation of transcription by distal elements. Future experiments informed by our model may be able to control contact probabilities within genomic sections of interest.

Materials and Methods

Hybrid MD–MC simulations were used to model active loop extrusion on linear polymer chains. Chains in theta-like solvent were simulated using the Kremer–Grest bead-spring model (76). A finite extensible nonlinear elastic (FENE) potential connected bonded beads. Nonbonded beads interact via a shifted and truncated Lennard-Jones pairwise potential. We represent cohesin as a switchable FENE bond that can move between binding partners. The FENE bond representing cohesin changes partners according to MC. The spatial trajectories of each bead were evolved in time by MD. Cohesin binding and translocation kinetics were updated by MC. MD was performed using the Large-scale Atomic/Molecular Massively Parallel Simulator package (77). MC steps were implemented in C and coupled to MD. For most simulations, chains were initiated as random walks and equilibrated for at least ten times their relaxation times before starting extrusion. At least 100 replicates were run of each condition for single extrusion cycle simulations. The steady-state simulations were run for at least 10 times the end-to-end vector autocorrelation decay time. Contact probabilities in steady-state simulations are consistent across different initial chain conformations (*SI Appendix*). Experimental contact probability plots were extracted from Micro-C data using cooltools (78). See *SI Appendix* for extended methods.

Data, Materials, and Software Availability. Simulation code can be found at https://doi.org/10.5281/zenodo.11118363 (79). All other study data are included in the article and/or *SI Appendix*.

ACKNOWLEDGMENTS. M.R. acknowledges funding support by the NSF under grant number EFMA-1830957 and the NIH under grant numbers P01-HL164320 and 5P01-HL108808.

1. S. Schoenfelder, P. Fraser, Long-range enhancer–promoter contacts in gene expression control. *Nat. Rev. Genet.* **20**, 437–455 (2019).
2. O. Symmons *et al.*, The Shh topological domain facilitates the action of remote enhancers by reducing the effects of genomic distances. *Dev. Cell* **39**, 529–543 (2016).
3. O. Symmons *et al.*, Functional and topological characteristics of mammalian regulatory domains. *Genome Res.* **24**, 390–400 (2014).
4. F. Sun *et al.*, Promoter–enhancer communication occurs primarily within insulated neighborhoods. *Mol. Cell* **73**, 250–263.e5 (2019).
5. W. Schwarzer *et al.*, Two independent modes of chromatin organization revealed by cohesin removal. *Nature* **551**, 51–56 (2017).
6. J. R. Dixon *et al.*, Topological domains in mammalian genomes identified by analysis of chromatin interactions. *Nature* **485**, 376–380 (2012).
7. G. Fudenberg *et al.*, Formation of chromosomal domains by loop extrusion. *Cell Rep.* **15**, 2038–2049 (2016).
8. A. L. Sanborn *et al.*, Chromatin extrusion explains key features of loop and domain formation in wild-type and engineered genomes. *Proc. Natl. Acad. Sci. U.S.A.* **112**, E6456–E6465 (2015).
9. E. Alipour, J. F. Marko, Self-organization of domain structures by DNA-loop-extruding enzymes. *Nucleic Acids Res.* **40**, 11202–11212 (2012).
10. K. Nasmyth, Disseminating the genome: Joining, resolving, and separating sister chromatids during mitosis and meiosis. *Annu. Rev. Genet.* **35**, 673–745 (2001).
11. B. Chan, M. Rubinstein, Theory of chromatin organization maintained by active loop extrusion. *Proc. Natl. Acad. Sci. U.S.A.* **120**, e2222078120 (2023).
12. E. J. Banigan, A. A. van den Berg, H. B. Brandão, J. F. Marko, L. A. Mirny, Chromosome organization by one-sided and two-sided loop extrusion. *Elife* **9**, e53558 (2020).
13. S. C. Weber, A. J. Spakowitz, J. A. Theriot, Nonthermal ATP-dependent fluctuations contribute to the in vivo motion of chromosomal loci. *Proc. Natl. Acad. Sci. U.S.A.* **109**, 7338–7343 (2012).
14. D. Saintillan, M. J. Shelley, A. Zidovska, Extensile motor activity drives coherent motions in a model of interphase chromatin. *Proc. Natl. Acad. Sci. U.S.A.* **115**, 11442–11447 (2018).
15. A. Zidovska, D. A. Weitz, T. J. Mitchison, Micron-scale coherence in interphase chromatin dynamics. *Proc. Natl. Acad. Sci. U.S.A.* **110**, 15555–15560 (2013).
16. K. Liu, A. E. Patteson, E. J. Banigan, J. M. Schwarz, Dynamic nuclear structure emerges from chromatin cross-links and motors. *Phys. Rev. Lett.* **126**, 158101 (2021).
17. P. Cramer, Organization and regulation of gene transcription. *Nature* **573**, 45–54 (2019).
18. J. Rodriguez, D. R. Larson, Transcription in living cells: Molecular mechanisms of bursting. *Annu. Rev. Biochem.* **89**, 189–212 (2020).
19. R. Phillips, J. Kondev, J. Theriot, H. G. Garcia, N. Orme, *Physical Biology of the Cell* (Garland Science, 2012), 10.1201/9781134111589.
20. X. Darzacq *et al.*, In vivo dynamics of RNA polymerase II transcription. *Nat. Struct. Mol. Biol.* **14**, 796–806 (2007).
21. M. D. Wang *et al.*, Force and velocity measured for single molecules of RNA polymerase. *Science* **282**, 902–907 (1998).
22. I. F. Davidson *et al.*, DNA loop extrusion by human cohesin. *Science* **366**, 1338–1345 (2019).
23. S. Golfier, T. Quail, H. Kimura, J. Brugués, Cohesin and condensin extrude DNA loops in a cell-cycle dependent manner. *Elife* **9**, 1–34 (2020).
24. Y. Kim, Z. Shi, H. Zhang, I. J. Finkelstein, H. Yu, Human cohesin compacts DNA by loop extrusion. *Science* **366**, 1345–1349 (2019).
25. M. Cremer *et al.*, Cohesin depleted cells rebuild functional nuclear compartments after endomitosis. *Nat. Commun.* **11**, 1–16 (2020).
26. N. Krietenstein *et al.*, Ultrastructural details of mammalian chromosome architecture. *Mol. Cell* **78**, 554–565.e7 (2020).
27. S. Zhang, N. Übelmesser, M. Barbieri, A. Papantonis, Enhancer–promoter contact formation requires RNAPII and antagonizes loop extrusion. *Nat. Genet.* **55**, 832–840 (2023).
28. E. Lieberman-Aiden *et al.*, Comprehensive mapping of long-range interactions reveals folding principles of the human genome. *Science* **326**, 289–293 (2009).
29. B. J. H. Dequeker *et al.*, MCM complexes are barriers that restrict cohesin-mediated loop extrusion. *Nature* **606**, 197–203 (2022).
30. T. H. S. Hsieh *et al.*, Resolving the 3D landscape of transcription-linked mammalian chromatin folding. *Mol. Cell* **78**, 539–553.e8 (2020).
31. Y. Liu, J. Dekker, CTCF–CTCF loops and intra-TAD interactions show differential dependence on cohesin ring integrity. *Nat. Cell Biol.* **24**, 1516–1527 (2022).
32. T. H. S. Hsieh *et al.*, Enhancer–promoter interactions and transcription are largely maintained upon acute loss of CTCF, cohesin, WAPL or YY1. *Nat. Genet.* **54**, 1919–1932 (2022).
33. J. D. Halverson, J. Smrek, K. Kremer, A. Y. Grosberg, From a melt of rings to chromosome territories: The role of topological constraints in genome folding. *Rep. Prog. Phys.* **77**, 022601 (2014).
34. M. Rubinstein, R. Colby, *Polymer Physics* (Oxford University Press, ed. 1, 2003), 10.1007/978-3-7091-0670-9.
35. S. S. P. Rao *et al.*, A 3D map of the human genome at kilobase resolution reveals principles of chromatin looping. *Cell* **159**, 1665–1680 (2014).
36. H. S. Long *et al.*, Making sense of the linear genome, gene function and TADs. *Epigenetics Chromatin* **15**, 4 (2022).
37. S. S. P. Rao *et al.*, Cohesin loss eliminates all loop domains. *Cell* **171**, 305–320.e24 (2017).
38. I. Robles-Rebollo *et al.*, Cohesin couples transcriptional bursting probabilities of inducible enhancers and promoters. *Nat. Commun.* **13**, 1–16 (2022).
39. J. M. Luppino *et al.*, Cohesin promotes stochastic domain intermingling to ensure proper regulation of boundary-proximal genes. *Nat. Genet.* **52**, 840–848 (2020).
40. Q. Szabo *et al.*, Regulation of single-cell genome organization into TADs and chromatin nanodomains. *Nat. Genet.* **52**, 1151–1157 (2020).
41. Q. Szabo *et al.*, TADs are 3D structural units of higher-order chromosome organization in Drosophila. *Sci. Adv.* **4**, eaar8082 (2018).
42. A. Rosa, R. Everaers, Structure and dynamics of interphase chromosomes. *PLoS Comput. Biol.* **4**, 1000153 (2008).
43. D. Jost, A. Rosa, C. Vaillant, R. Everaers, A polymer physics view on universal and sequence-specific aspects of chromosome folding. *Nucl. Archit. Dyn.* **2**, 149–169 (2018).
44. K. E. Polovnikov *et al.*, Crumpled polymer with loops recapitulates key features of chromosome organization. *Phys. Rev. X* **13**, 041029 (2023).
45. F. Tavares-Cadete, D. Norouzi, B. Dekker, Y. Liu, J. Dekker, Multi-contact 3C reveals that the human genome during interphase is largely not entangled. *Nat. Struct. Mol. Biol.* **27**, 1105–1114 (2020).
46. K. Polovnikov, B. Slavov, Topological and nontopological mechanisms of loop formation in chromosomes: Effects on the contact probability. *Phys. Rev. E* **107**, 054135 (2023).
47. T. Ge, S. Panyukov, M. Rubinstein, Self-similar conformations and dynamics in entangled melts and solutions of nonconcatenated ring polymers. *Macromolecules* **49**, 708–722 (2016).
48. A. Rosa, R. Everaers, Conformational statistics of randomly branching double-folded ring polymers. *Eur. Phys. J. E Soft Matter* **42**, 7 (2019).
49. M. Rubinstein, Dynamics of ring polymers in the presence of fixed obstacles. *Phys. Rev. Lett.* **57**, 3023–3026 (1986).
50. W. F. M. Daniel *et al.*, Solvent-free, supersoft and superelastic bottlebrush melts and networks. *Nat. Mater.* **15**, 183–189 (2016).
51. C. Cattoglio *et al.*, Determining cellular CTCF and cohesin abundances to constrain 3D genome models. *Elife* **8**, e40164 (2019).
52. A. Tedeschi *et al.*, Wapl is an essential regulator of chromatin structure and chromosome segregation. *Nature* **501**, 564–568 (2013).
53. A. S. Hansen, I. Pustova, C. Cattoglio, R. Tjian, X. Darzacq, CTCF and cohesin regulate chromatin loop stability with distinct dynamics. *Elife* **6**, e25776 (2017).
54. M. Gabriele *et al.*, Dynamics of CTCF- and cohesin-mediated chromatin looping revealed by live-cell imaging. *Science* **376**, 476–501 (2022).
55. I. Bronshtein *et al.*, Loss of lamin A function increases chromatin dynamics in the nuclear interior. *Nat. Commun.* **6**, 8044 (2015).
56. M. Socol *et al.*, Rouse model with transient intramolecular contacts on a timescale of seconds recapitulates folding and fluctuation of yeast chromosomes. *Nucleic Acids Res.* **47**, 6195–6207 (2019).
57. B. Gu *et al.*, Transcription-coupled changes in nuclear mobility of mammalian cis-regulatory elements. *Science* **359**, 1050–1055 (2018).
58. A. Jack *et al.*, Compartmentalization of telomeres through DNA-scaffolded phase separation. *Dev. Cell* **57**, 277–290.e9 (2022).
59. L. Stadler, M. Weiss, Non-equilibrium forces drive the anomalous diffusion of telomeres in the nucleus of mammalian cells. *New J. Phys.* **19**, 113048 (2017).
60. T. A. Kavassalis, J. Noolandi, New view of entanglements in dense polymer systems. *Phys. Rev. Lett.* **59**, 2674–2677 (1987).
61. A. Rohatgi, WebPlotDigitizer. GitHub. https://github.com/automeris-io/WebPlotDigitizer/. Deposited 16 September 2022.
62. D. B. Brückner, H. Chen, L. Barinov, B. Zoller, T. Gregor, Stochastic motion and transcriptional dynamics of pairs of distal DNA loci on a compacted chromosome. *Science* **380**, 1357–1362 (2023).
63. H. Ma *et al.*, Cell cycle– and genomic distance–dependent dynamics of a discrete chromosomal region. *J. Cell Biol.* **218**, 1467–1477 (2019).
64. N. Khanna, Y. Zhang, J. S. Lucas, O. K. Dudko, C. Murre, Chromosome dynamics near the sol-gel phase transition dictate the timing of remote genomic interactions. *Nat. Commun.* **10**, 2771 (2019).
65. L. Rinaldi *et al.*, The glucocorticoid receptor associates with the cohesin loader NIPBL to promote long-range gene regulation. *Sci. Adv.* **8**, eabj8360 (2022).
66. A. Hafner *et al.*, Loop stacking organizes genome folding from TADs to chromosomes. *Mol. Cell* **83**, 1377–1392.e6 (2023).
67. J. H. I. Haarhuis *et al.*, The cohesin release factor WAPL restricts chromatin loop extension. *Cell* **169**, 693–707.e14 (2017).
68. N. Q. Liu *et al.*, WAPL maintains a cohesin loading cycle to preserve cell-type-specific distal gene regulation. *Nat. Genet.* **53**, 100–109 (2021).
69. I. F. Davidson, J. M. Peters, Genome folding through loop extrusion by SMC complexes. *Nat. Rev. Mol. Cell Biol.* **22**, 445–464 (2021).
70. E. J. Banigan *et al.*, Transcription shapes 3D chromatin organization by interacting with loop extrusion. *Proc. Natl. Acad. Sci. U.S.A.* **120**, e2210480120 (2023).
71. S. Zhang *et al.*, RNA polymerase II is required for spatial chromatin reorganization following exit from mitosis. *Sci. Adv.* **7**, 8205–8227 (2021).
72. S. Leidescher *et al.*, Spatial organization of transcribed eukaryotic genes. *Nat. Cell Biol.* **24**, 327–339 (2022).
73. A. J. M. Larsson *et al.*, Genomic encoding of transcriptional burst kinetics. *Nature* **565**, 251–254 (2019).
74. J. Rodriguez *et al.*, Intrinsic dynamics of a human gene reveal the basis of expression heterogeneity. *Cell* **176**, 213–226.e18 (2019).
75. T. Cremer, C. Cremer, Chromosome territories, nuclear architecture and gene regulation in mammalian cells. *Nat. Rev. Genet.* **2**, 292–301 (2001).
76. K. Kremer, G. S. Grest, Dynamics of entangled linear polymer melts: A molecular-dynamics simulation. *J. Chem. Phys.* **92**, 5057–5086 (1990).
77. S. Plimpton, Fast parallel algorithms for short-range molecular dynamics. *J. Comput. Phys.* **117**, 1–42 (1997).
78. Open2C *et al.*, Cooltools: Enabling high-resolution Hi-C analysis in Python. bioRxiv [Preprint] (2022). https://doi.org/10.1101/2022.10.31.514564 (Accessed 10 December 2023).
79. B. Chan, Active loop extrusion simulation on a single polymer chain. Zenodo. https://doi.org/10.5281/zenodo.11118363. Deposited 6 May 2024.